nature chemical biology

SUPPLEMENTARY INFORMATION

https://doi.org/10.1038/s41589-018-0216-z

In the format provided by the authors and unedited.

Mechanism of regulation and neutralization of the AtaR–AtaT toxin–antitoxin system

Dukas Jurėnas[1,2], Laurence Van Melderen[1] and Abel Garcia-Pino[1,3]*

[1]Cellular and Molecular Microbiology, Department of Molecular Biology, Université Libre de Bruxelles, Gosselies, Belgium. [2]Department of Biochemistry and Molecular biology, Vilnius University Joint Life Sciences Center, Vilnius, Lithuania. [3]WELBIO, Brussels, Belgium. *e-mail: agarciap@ulb.ac.be

TITLE

Mechanism of regulation and neutralization of the AtaR-AtaT toxin-antitoxin system

Dukas Jurėnas[1], Laurence Van Melderen[1] and Abel Garcia-Pino[1,2*]

[1] Cellular and Molecular Microbiology, Department of Molecular Biology, Université Libre de Bruxelles

[2] WELBIO Avenue Hippocrate 75, 1200 Brussels, Belgium

SUPPLEMENTARY TABLES

Supplementary Table 1. Binding parameters obtained from the ITC titrations. The binding affinities were determined from fitting a single interaction model to the experimental ITC data according to the experimental setup (see the main text and the Supplementary Material and Methods for details). Data represent mean values ± s.d.

ITC Titration	**Kd**	**n**	**Exp.**
ac-CoA into $AtaT_{Y44F}$	245 ± 1 nM	0.92	3
ac-CoA into $AtaT_{V126D}$	306 ± 3 nM	1.0	2
$AtaT_{Y44F}$ into AtaR	29 ± 0.5 nM	0.97	2
$AtaR^{44-88}$ into $AtaT_{Y44F}$	367 ± 3 nM	1.1	3
$AtaR^{44-88}$ into $AtaT_{V126D}$	397 ± 1 nM	0.91	2
$AtaR^{60-88}$ into $AtaT_{Y44F}$	862 ± 8 nM	0.9	3
CoA into $AtaT_{Y44F}$	491 ± 3 nM	0.93	3
ac-CoA into AtaR-$AtaT_{Y44F}$	873 ± 7 nM	1.0	2
ac-CoA-$AtaT_{Y44F}$ into Met-$tRNA^{fMet}$	2 ± 10 µM	0.91	2
AtaR-AtaT into Operator DNA	176 ± 5 nM	1.0	2
$AtaT_{Y44F}$ into AtaR-AtaT	445 ± 5 nM	1.2	2

Supplementary Table 2. Oligonucleotides used for cloning, mutagenesis and T7-transcription, ITC and crystallization. Underlined – restriction sites, minor case – substitutions, bold AtaT binding boxes.

Oligonucleotides used for cloning	
F-Pata-SacI	GATCGAGCTCTTTGTGTTTGTCGAAATGGTTGTA
R-Pata-BamHI	GATCGGATCCGTGAACTCTCCTGCTCCGTA
F-AtaR-Eco	GATCGAATTCATGTCTGCTGTTAAAAAGCAG
R-AtaR-Hind	GATCAAGCTTTTACATTCCCTGAAGACGTTT
R-AtaT-Hind	GATCAAGCTTTTAATCGCTCTGTGTAAAAAGCA
R-AtaR-3-Hind	GATCAAGCTTTTAAAGACGTTTTGCCGCACGTT
R-AtaR-6-Hind	GATCAAGCTTTTATGCCGCACGTTTTAGCTTTT
R-AtaR-9-Hind	GATCAAGCTTTTATTTTAGCTTTTCACCTGGTGACG
Oligonucleotides used for mutagenesis	
F-AtaT-SL146-7HH	CACCATGGCTTTATCCCTTTAGTCGG
R-AtaT-S146	TTTATAAAACGTATGGGCTTTTT
R-AtaT-R45	CAGAATTTTGTTGCGATGTT
F-AtaT-R45A	gcgGCGTATATCCTTTGTCGCAA
F-AtaT-R45E	gaaGCGTATATCCTTTGTCGCAA
R-AtaT-R71	TTCAAAACAACTGCCGCAT
F-AtaT-R71A	gcgGCCGCATTGCCCTCGAAA
F-AtaT-R71E	gaaGCCGCATTGCCCTCGAAA
R-AtaT-K86	GTAGGGAATTTTTTTCTGTTTCGA
F-AtaT-K86A	gcgAATATTCCCAGCGTTACTC
F-AtaT-K86E	gaaAATATTCCCAGCGTTACTC
R-AtaT-H129	AATACCTACCGCTAAAGAGG
F-AtaT-H129A	gcgGGTCTTTTTGTCGAGGCG
F-AtaT-H129E	gaaGGTCTTTTTGTCGAGGCG
R-AtaT-K165	GGTTGGGAAAAATAACGCAT
F-AtaT-K165A	gcgTCCATTGAACTGCTTTTTACAC
F-AtaT-K165E	gaaTCCATTGAACTGCTTTTTACAC
R-AtaT-S101	ACGATCAATTGCCAGACG
F-AtaT-S101A	gcgTTACAGGGGCAGGGATGG
F-AtaT-S101E	gaaTTACAGGGGCAGGGATGG
R-AtaT-H141	GGCTTTTTCATTCAGCGC
F-AtaT-H141A	gcgACGTTTTATAAATCGCTGGG
F-AtaT-H141E	gaaACGTTTTATAAATCGCTGGG
F-AtaT-V126D	gatGGTATTCACGGTCTTTTTGTCG

R-AtaT-V126	CGCTAAAGAGGCTGACCAG
F-AtaT-A122W	tggTCTTTAGCGGTAGGTATTCACG
F-AtaT-A122Y	tatTCTTTAGCGGTAGGTATTCACG
R-AtaT-A122	TGACCAGACGACGTTCATGG
F-AtaR-K6A	gcgCAGCGTATCGATCTGCGTT
R-AtaR-K6	TTTAACAGCAGACATAGACTGGAAG
F-AtaR-R8A	gcgATCGATCTGCGTTTAACTGAC
R-AtaR-R8	CTGCTTTTTAACAGCAGACATAGA
F-AtaR-D10A	gcgCTGCGTTTAACTGACGATGAC
R-AtaR-D10	GATACGCTGCTTTTTAACAGC
F-AtaR-D12A	gcgTTAACTGACGATGACAAAAGTATGAT
R-AtaR-D12	CAGATCGATACGCTGCTTTTT
F-AtaR-K18G	ggcAGTATGATTGAGGAAGCGGC
R-AtaR-K18	GTCATCGTCAGTTAAACGCAG
F-AtaR-V64D	gatATGGATGCGCTGAGTAATCC
R-AtaR-V64	CCGCGTCCAGGATTCCTCA
F-AtaR-L68D	gatAGTAATCCACCGTCACCAGG
R-AtaR-L68	CGCATCCATCACCCGCGTC
Oligonucleotides used for amplifying T7-transcription templates for *in vitro* transcription-translation assays	
5'UTR-fullC	GCGAATTAATACGACTCACTATAGGGCTTAAGTATAAGGAGGAAAAAATATGGCTGCGGAAGTGATTGAAC
5'UTR-50	GCGAATTAATACGACTCACTATAGGGCTTAAGTATAAGGAGGAAAAAATATGCAGCATCGGCGGGTGATCCTCA
5'UTR-60	GCGAATTAATACGACTCACTATAGGGCTTAAGTATAAGGAGGAAAAAATATGTCCTGGACGCGGGTGATGGA
5'UTR-70	GCGAATTAATACGACTCACTATAGGGCTTAAGTATAAGGAGGAAAAAATATGAATCCACCGTCACCAGGTGA
5'UTR-80	GCGAATTAATACGACTCACTATAGGGCTTAAGTATAAGGAGGAAAAAATATGCGTGCGGCAAAACGTCTTC
3'UTR-AtaR	AAACCCCTCCGTTTAGAGAGGGGTTATGCTAGTTATTACATTCCCTGAAGACGTTTTGC
3'UTR-ter60	AAACCCCTCCGTTTAGAGAGGGGTTATGCTAGTTATTAGGATTCCTCATTGAGGATCACC
3'UTR-ter70	AAACCCCTCCGTTTAGAGAGGGGTTATGCTAGTTATTAATTACTCAGCGCATCCATCACC
3'UTR-ter80	AAACCCCTCCGTTTAGAGAGGGGTTATGCTAGTTATTAACGTTTTAGCTTTTCACCTGGT
Oligonucleotides used for EMSA	
Opr_{47}	**ATGTACGGT**GACAT**ACCGTACAT**ATTATACGGAGCAGGAGAGTTCAC

R- Opr_{47}	GTGAACTCTCCTGCTCCGTATAAT**ATGTACGGT**ATGTC**ACCGTACAT**
mut- Opr_{47}	**ATGTAttcT**GACAT**AgaaTACAT**ATTATACGGAGCAGGAGAGTTCAC
R-mut- Opr_{47}	GTGAACTCTCCTGCTCCGTATAAT**ATGTAttcT**ATGTC**AgaaTACAT**
Oligonucleotides used for ITC	
Opr_{22}	**ATGTACGGT**ATAT**ACCGTACAT**
Opr_{22}-C6T	**ATGTAtGGT**ATAT**ACCaTACAT**
Random	ATGTCTGCTGTTAAAAAGCAGCGTA
Oligonucleotides used for T7 synthesis of tRNAfMet	
Fmet	ATGTAATACGACTCACTATAGGCGGGGTGGAGCAGCCTGGTAGCTCGTCGGGCTCAT AACCCGAAGGTCGTCGGTTCAAATCCGGCCCCCGCAACCA
asFmet	TGGTTGCGGGGGCCGGATTTGAACCGACGACCTTCGGGTTATGAGCCCGACGAGCTA CCAGGCTGCTCCACCCCGCCTATAGTGAGTCGTATTACAT

Supplementary Table 3: SAXS parameters. Theoretically and experimentally determined SAXS parameters of the different species. The quality of the SAXS-based models was assessed based on the metrics recently proposed by Rambo and Tainer. Theoretical and calculated values are shown in brackets.

Sample	***Rg* (Å)**	D_{max} **(Å)**	**MW (kDa)**	χ^2	V_P (**Å^3**)	$\mathbf{V_C}$	$\mathbf{R_{SAS}}$	**Ensemble composition**
AtaR-AtaT complex	34.3 (34.8)	109.5	77.0 (78.5)	1.66	1.8	569.6 (538.8)	0.0035	4

Supplementary Table 4: Analysis of flow cytometry data. *E. coli* DJ624Δara cells expressing GFP-LVA from the P*ata* promoter co-transformed with *ataR* or *ataRT* and its mutated derivatives in pBAD24 vector. Cells were grown in liquid M9 medium and protein expression from pBAD24 was induced by addition of 0.2% arabinose at exponential phase. Data from 40 000 cells after 1 hour of AtaR or AtaRT induction was analysed using Flow Jo software. Cells carrying pPROBE-GFP-LVA vector without any promoter in front of GFP-LVA served as a control to select the gate for fluorescence analysis. Low fluorescence in this analysis is under 1000 A.U, high fluorescence – above 1000 A.U.

	pPROBE_ GFP-LVA	Pata	Pata_ AtaR	Pata_ AtaRT	Pata_ $AtaR_{K6A}$-AtaT	Pata_ $AtaR_{R8A}$-AtaT	Pata_ $AtaR_{D10A}$-AtaT	Pata_ $AtaR_{R12A}$-AtaT	Pata_ $AtaR_{K18G}$-AtaT	Pata_ $AtaR_{L68D}$-AtaT
% high fluo	0	94.2	96.2	1.11	20.4	55	89.6	92.5	83.6	97.9
% low fluo	100	5.76	3.8	98.9	79.6	45	10.4	7.53	16.4	2.13

Supplementary Table 5. Data collection and processing. Values for the outer shell are given in parentheses.

Sample	Sel-Met AtaR	AtaR	$AtaT_{Y144F}$-$AtaR_{44-86}$	$AtaT_{Y144F}$	$AtaT_{Y144F}$-$AtaR_{44-86}$-ac-CoA	AtaT-AtaR-DNA complex
Data collection						
Space group	$P6_122$	$P6_122$	$P3_121$	$P6_522$	$P3_121$	$C222_1$
a, *b*, *c* (Å)	56.3, 56,3 160.8	56.0, 56.0, 165.8	87.6, 87.6, 125.5	58.1, 58.1, 216.7	87.9 87.9 125.6	75.6, 87.9, 190.5
α, β, γ (°)	90.0, 90.0, 120.0	90.0, 90.0, 120.0	90.0, 90.0, 120.0	90.0, 90.0, 120.0	90.0, 90.0, 120.0	90.0, 90.0, 90.0
Resolution range (Å)	46.64 – 3.78 (3.92 – 3.78)	41.86 – 2.97 (3.08 – 2.97)	50.00 – 2.29 (2.35 – 2.29)	45.54 – 2.49 (2.55 – 2.51)	41.87 – 2.99 (3.11 - 2.99)	95.24 - 3.58 (3.64 – 3.58)
Completeness (%)	99.4 (95.2)	99.61 (99.42)	99.3 (90.6)	100 (100)	99.9 (99.8)	91.0 (93.8)
Redundancy	34.8 (32.5)	5.5 (4.2)	10.8 (9.6)	12.2 (13.1)	6.7 (6.4)	7.3 (6.6)
$\langle I/\sigma(I)\rangle$	9.2 (1.6)	9.58 (0.44)	12.1 (0.8)	8.6 (0.6)	31.0 (9.9)	8.9 (0.8)
$CC_{1/2}$	0.999 (0.552)	1 (0.538)	0.998 (0.324)	0.998 (0.448)	0.999 (0.998)	0.998 (0.352)
$R_{r.i.m.}$	0.148 (1.423)	0.05645 (1.482)	0.065 (1.321)	0.056 (1.520)	0.085 (0.30)	0.040 (0.863)
Refinement						
N°. of unique reflections	1776 (197)	3575 (341)	25564 (1688)	8089 (376)	11678 (1831)	7075 (354)
R-factor (%)	–	0.234 (0.411)	0.196 (0.319)	0.196 (0.328)	0.199 (0.233)	0.266 (0.392)
R_{free}-factor (%)	–	0.266 (0.406)	0.236 (0.340)	0.254 (0.484)	0.266 (0.316)	0.289 (0.467)
Ramachandran profile						
Core	–	100.0	95.8	95.5	96.0	94.5
Allowed	–	0.0	4.2	4.5	4.0	5.1
Outliers	–	0.0	0.0	0.0	0.0	0.4
R.m.s. deviations						
Bond lengths (Å)	–	0.015	0.016	0.013	0.018	0.009
Bond angles (o)	–	1.70	1.78	1.96	1.81	1.45
Number of atoms	–	464	3314	1474	3121	2659
Macromolecules	–	460	3035	1378	3029	2659
Solvent	–	0	214	42	34	0
Other	–	4	65	54	58	0
B-factors (Å2)						
All atoms	–	134.3	66.3	62.2	58.1	156.0
Macromolecules	–	134.3	66.0	63.0	57.5	156.0
Solvent atoms	–	–	65.4	58.0	44.3	–

Other atoms	–	–	85.3	44.6	99.3	–
PDB ID		6GTO	6GTQ	6GTP	6GTR	6GTS

SUPPLEMENTARY FIGURES

Supplementary Fig. 1. Structure of AtaT$_{Y144F}$. (a) *In vitro* acetylation reactions of a tRNA mixture purified from *E. coli* supplemented with [14C]ac-CoA. Reaction products were resolved by native PAGE and stained with methylene blue (top panel) and exposed to phosphor storage screen (bottom panel). (**b**) Molecular surface model of AtaT$_{Y144F}$ bound to ac-CoA. The surface is coloured as in Fig. 1d. The ac-CoA molecule bound to AtaT$_{Y144F}$ is shown as sticks and binds in a predominantly positive patch that accommodates the phosphate groups of ac-CoA. (**c**) Structure of the AtaT$_{Y144F}$-ac-CoA complex (shown in light blue) superimposed on the complex of TacT-ac-CoA (shown in pink) and the complex of KacT-ac-CoA (shown in yellow). From the comparison it becomes apparent that the substitutions in α–helix α3 result in the binding site exchange of the phosphate group and the adenosine base of ac-CoA with respect to AtaT. (**d**) Ten fold serial dilutions of overnight cultures of *E. coli* strains transformed with pBAD33 vector or derivatives encoding *ataT*, or the *ataT* mutants *ataT$_{Y144F}$*, *ataT$_{S146H/L147H}$*, and *ataT$_{G108T}$* under repression or induction conditions. The assay shows that while substitutions affecting ac-CoA binding such as G108T render the toxin inactive[7], after the double S146H/L147H substitution that flips the adenine base of ac-CoA, AtaT remains toxic, suggesting the that the stabilization of the group rather than the orientation, is important for catalysis. (**e**) Large cleft (shown in green) formed at the dimer interface of AtaT. This cavity defines a large positive surface involving residues R71, K79, K86, H129 and K165 of one monomer; together with H34, R37, Q38, R40, R45 and R95 (as shown in **Fig. 1d**). From the interface, it leads directly towards the catalytic Y144 and the site where the acetyl group of ac-CoA is bound (highlighted by a red arrow). (**f**) SEC profiles of AtaT$_{Y144F}$ and AtaT$_{V126D}$. The comparison of the retention volumes of both versions of AtaT shows that the V126D substitution precludes the dimerization. (**g**) Western blotting of the SEC purified AtaT$_{Y144F}$ and AtaT$_{V126D}$ fractions. (**h**) Ten-fold dilutions of overnight cultures of *E. coli* strains transformed with pBAD33 vector or derivatives expressing AtaT, or the *ataT* mutants *ataT$_{Y144F}$* and *ataT$_{V126D}$* under repression or induction conditions. The assay shows that the V126D substitution is not toxic.

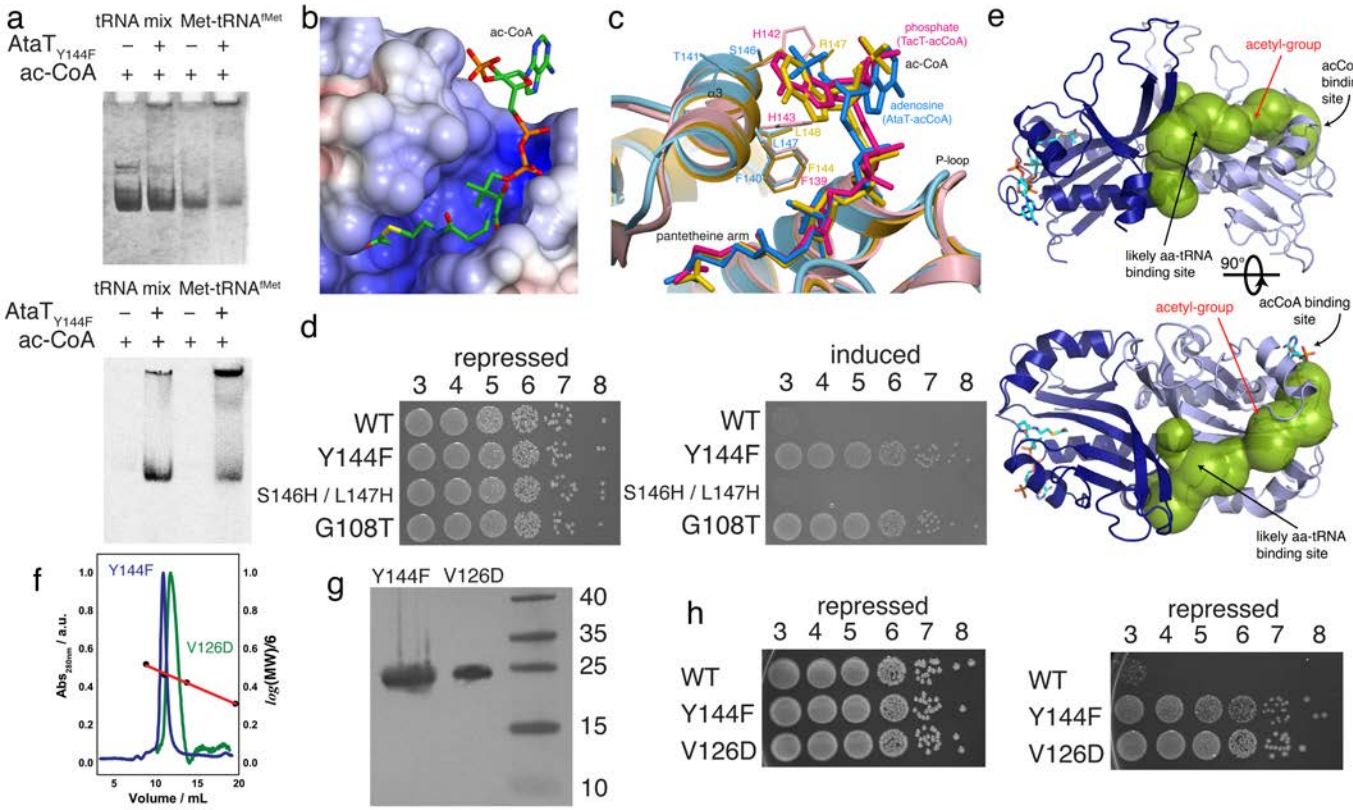

Supplementary Fig. 2. ITC measurements. Titration of ac-CoA into AtaT$_{Y144F}$ (**a**), CoA into AtaT$_{Y144F}$ (**b**), Met-tRNA^{fMet} into ac-CoA-AtaT$_{Y144F}$ (**c**), tRNA^{fMet} into ac-CoA-AtaT$_{Y144F}$ (**d**), (**e**) Far UV CD spectrum of AtaT$_{Y144F}$ in red and AtaT$_{V127D}$ in red. Both CD spectra display the typical minimal at around 210 nm and 220 nm observed in proteins that contain α–helices. (**f**) ac-CoA into AtaT$_{V127D}$, (**g**) AtaT$_{Y144F}$ into AtaR, (**h**) AtaR$^{A44\text{-}M88}$ into AtaT$_{Y144F}$ (**i**), AtaR$^{S60\text{-}M88}$ into AtaT$_{Y144F}$, (**j**) AtaR$^{A44\text{-}M88}$-AtaT$_{Y144F}$ into Met-tRNA^{fMet}, (**k**) ac-CoA into AtaR-AtaT$_{Y144F}$, (**l**) AtaT$_{Y144F}$ into AtaR-AtaT, (**m**) AtaR-AtaT into Opr$_{22}$, (**n**) AtaR$^{A44\text{-}M88}$ into AtaT$_{V127D}$, (**o**) AtaR-AtaT into random DNA of 22bp, (**p**) AtaR-AtaT into Opr$_{22}^{C6T}$. Affinities (in the form of Kd) are shown in the inset.

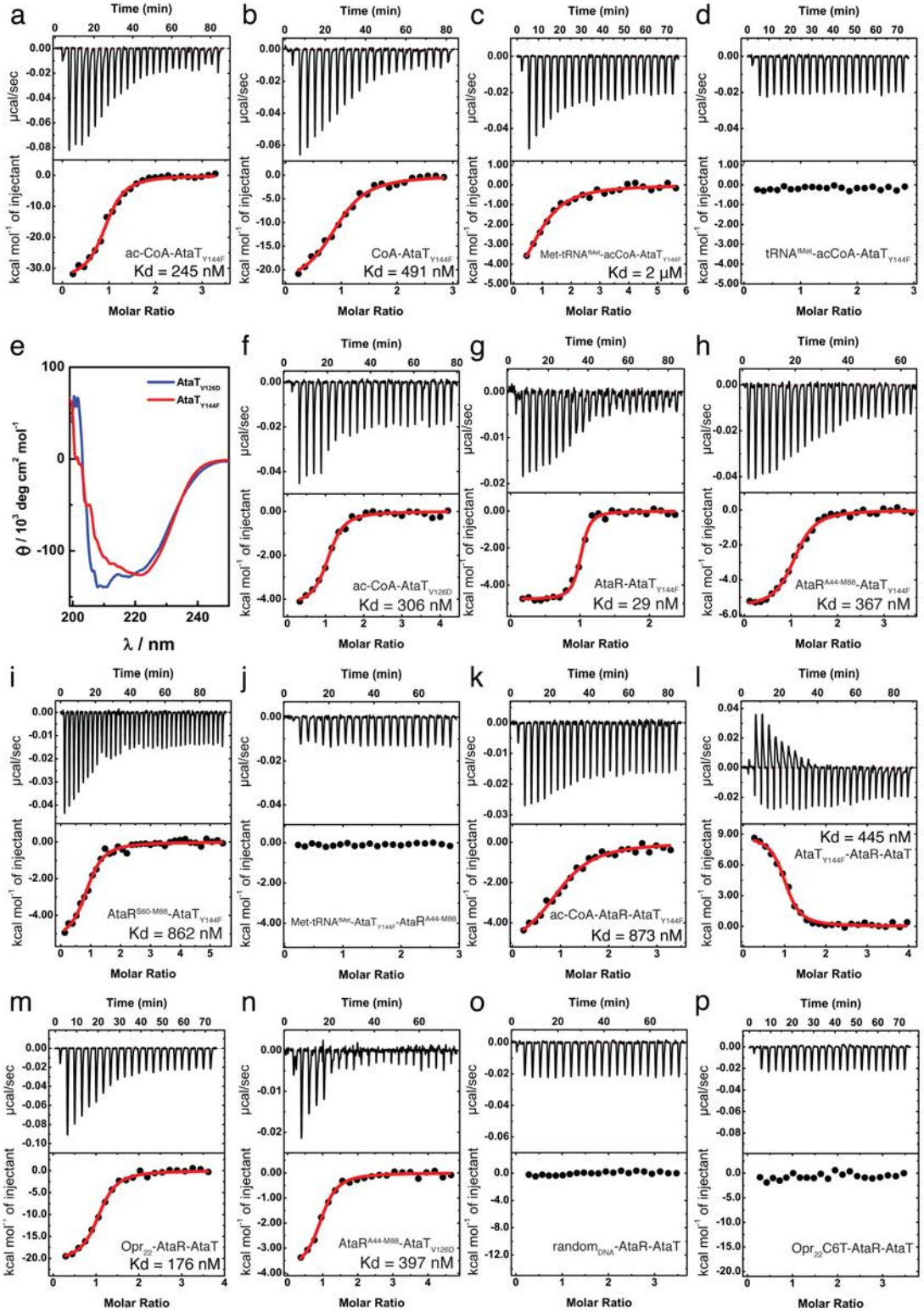

Supplementary Fig. 3. Structure of AtaR and AtaR$^{A44-M88}$ bound to AtaT$_{Y144F}$. (**a**) Crystal lattice packing of the P6$_1$22 crystal form of AtaR. The AtaR dimer is shown in blue and light blue with other symmetry related structures shown in raspberry. Black circles highlight the lattice contacts that stabilise the C-terminal α–helix of AtaR. (**b**) Far UV CD spectrum of AtaR in red. The spectrum of AtaR shows the typical minima at 210 nm and 220 nm expected for an α–helical protein. This is consistent with the large α–helical content of a protein with an RHH fold, as observed in the crystal structure. The CD spectrum of the isolated AtaR$^{A44-M88}$ (blue) and AtaR$^{S60-M88}$ (orange) are characteristic of an intrinsically disordered protein with a weak minimum around 205 nm. The inset show the comparison of the thermal denaturation of AtaR (in red) and AtaR$^{A44-M88}$ (in blue). As expected from the CD spectrum taken at 25°C, AtaR shows a thermal transition at around 42°C whereas AtaR$^{A44-M88}$, an IDR, lacks any transition. (**c**) Serial dilutions of overnight cultures of *E. coli* strains transformed with pBAD33 expressing *ataT* and the pKK223-3 vector expressing *ataR* or the deletions ataR$^{A44-M88}$, ataR$^{S60-M88}$, ataR^{M1-M85}, ataR^{M1-A82}, ataR^{M1-K79}, under repression or induction conditions. The assay shows that the deletion of the last 6 residues of AtaR already has a significant impact on the neutralization activity of the protein whereas the S60-M88 while able to inhibit AtaT *in vitro*, fails to neutralize the toxin *in vivo*. (**d**) Electron density map representation (unbiased mFo-DFc), of the AtaR$^{A44-M88}$ (coloured in raspberry) bound to AtaT$_{Y144F}$ (in cyan), after refinement with Buster/TNT. The map was calculated from the MR solution omitting the AtaR$^{A44-M88}$ peptide.

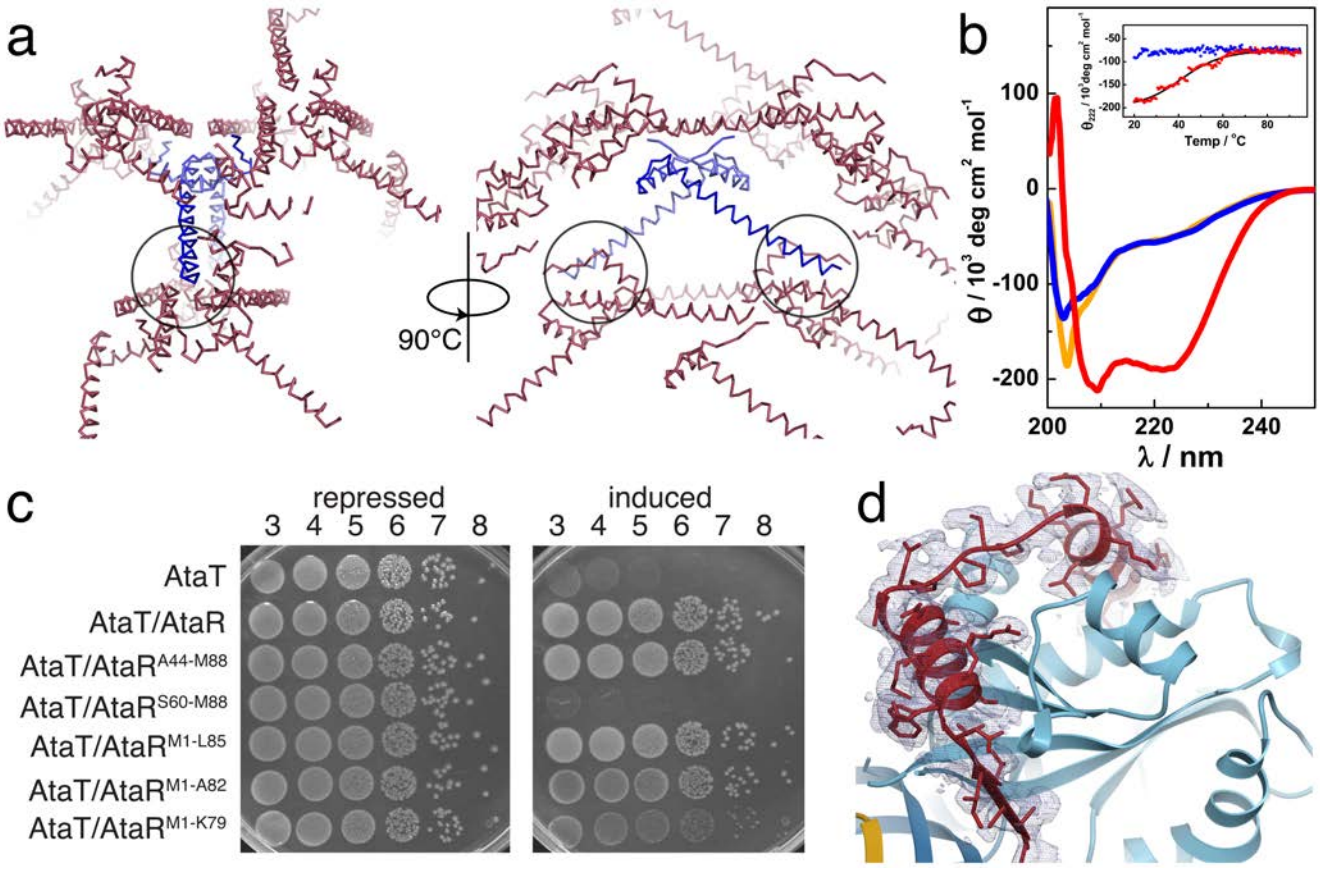

Supplementary Fig. 4. Structure of ac-CoA bound to the AtaR$^{A44\text{-}M88}$-AtaT$_{Y144F}$ complex. (**a**) Structure of AtaR$^{A44\text{-}M88}$-AtaT$_{Y144F}$ bound to ac-CoA. Ac-CoA as observed in the crystal structure of the AtaT$_{Y144F}$-ac-CoA complex is superimposed on the structure (shown in pink). The black arrow shows the ~ 180° flip of the pantetheine arm of ac-CoA that results from the presence of AtaR$^{A44\text{-}M88}$. (**b**) Unbiased mFo-DFc electron density map of the ac-CoA bound to the AtaR$^{A44\text{-}M88}$-AtaT$_{Y144F}$ complex, after refinement with Buster/TNT (and omitting ac-CoA).

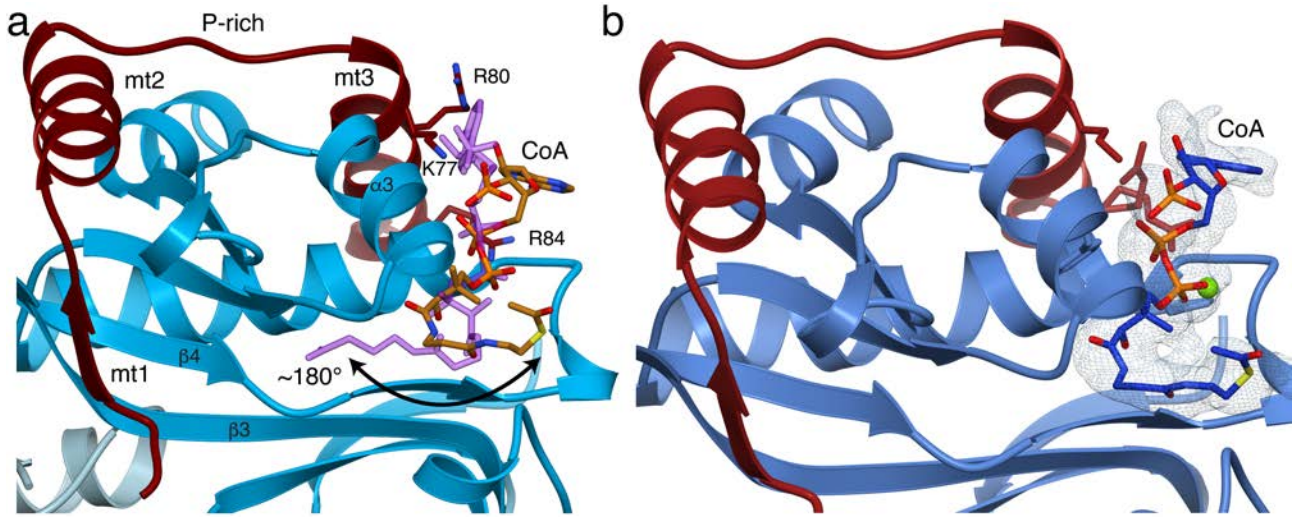

Supplementary Fig. 5. AtaT does not interact with Opr_{47}. EMSA assay to test whether or not AtaT interacts on its own with Opr_{47}. The assay shows that the toxin is unable to interact with DNA in the absence of AtaR.

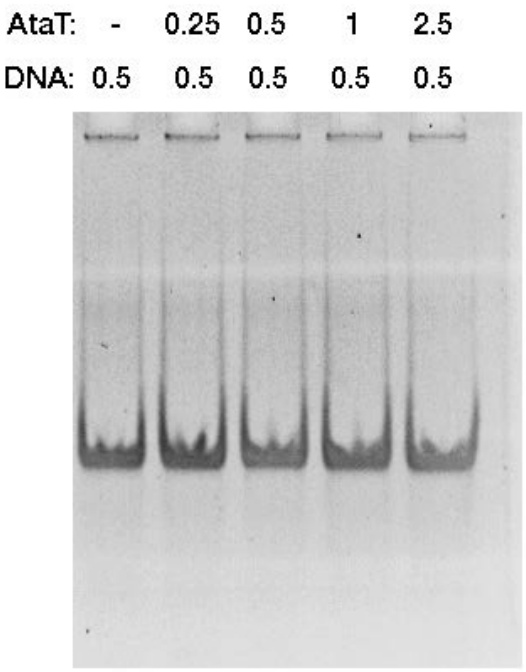

Supplementary Fig. 6. Structure of the AtaT−AtaR$_2$−Opr$_{22}$−AtaR$_2$−AtaT complex. (**a**) Unbiased mFo-DFc electron density map after refinement with Buster/TNT from the MR solution omitting the DNA is shown as a blue mesh. (**b**) Schematic illustration of the interactions observed in the AtaT−AtaR$_2$−Opr$_{22}$−AtaR$_2$−AtaT complex. The AtaR-binding box is highlighted by a light red rectangle. In the repressor complex, the antitoxin IDR interacts with the toxin at a second site, placing the DNA-binding domains of AtaR ~40 Å apart, matching the distance between the two GTAC binding boxes. The dimensions of this rhomboid structure are determined by α–helices α1 and α2 of AtaR. The black dot at the center of the complex represents the two-fold symmetry axis of the repressor complex. (**c**) Experimental SAXS data from AtaR$_2$−AtaT−AtaT−AtaR$_2$ (black circles), the theoretical scattering data calculated from the AtaR$_2$−AtaT−AtaT−AtaR$_2$ structural model (red curve) is superimposed on the experimental data. (**d**) Structure of the heterohexameric AtaR$_2$−AtaT−AtaT−AtaR$_2$ complex (as observed in the crystal structure of AtaT−AtaR$_2$−Opr$_{22}$−AtaR$_2$−AtaT) superimposed on the ab initio envelope calculated from the experimental SAXS data using DAMMIF. (**e**) SEC-MALS characterisation of the AtaR-AtaT complex. The analysis of the data indicates the complex has a molecular weight of around 83 kDa consistent with a hetero-hexameric stoichiometry, in agreement with the SEC-SAXS data shown in panel c. (**f**) Low resolution SAXS-based model of the AtaR$_2$−AtaT−AtaT−AtaR$_2$ showing that when the complex is not bound to DNA it contains large regions that are disordered.

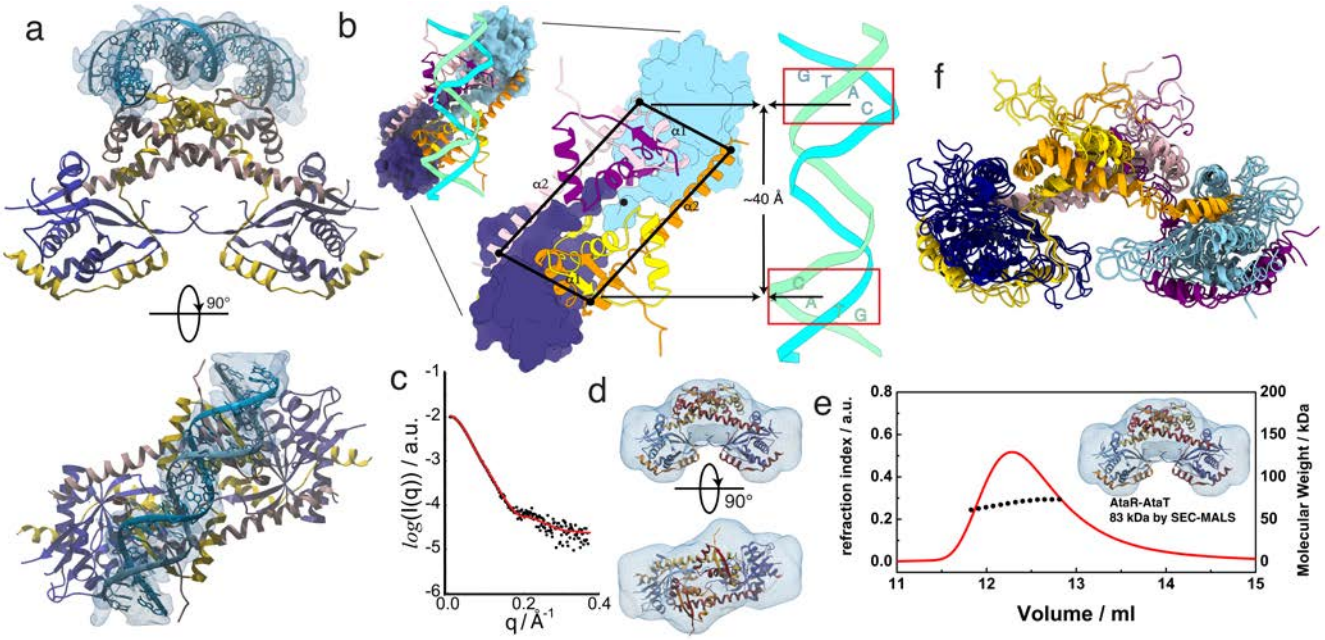

Supplementary Figure 7. Transcriptional regulation of ataRT promoter (P_{ata}) by AtaR and AtaRT. (**a**) Left panel – auto-fluorescence of *E. coli* DJ624Δara cells transformed with pPROBE-gfp-lva vector. Right panel – fluorescence from P_{ata} promoter cloned in front of gfp-lva in pPROBE-Pata-gfp-lva. Cells containing pPROBE vectors were co-transformed with pBAD24 (green curve), pBAD24-AtaR (blue curve) and pBAD24-AtaRT (red curve). Overnight cultures were diluted to OD_{600} = 0.02 (time 0) in M9 media with 0.2% glc and grown in SpectraMax microplate reader with constant shaking at 37 °C following OD at 600 nm and GFP fluorescence (485/520 nm). At early exponential phase (after 3h) expression of AtaR or AtaRT from pBAD24 was induced with 0.2% arabinose. OD_{600} and fluorescence intensity was further monitored for a total of 12 hours. Fluorescence intensity was normalised by OD_{600}. Curves represent three independent experiments; error bars indicate standard deviation. (**b**) Flow cytometry of *E. coli* DJ624Δara cells expressing GFP-LVA from the P*ata* promoter. The graph shows the GFP-LVA fluorescence of 40 000 cells after 1 hour of induction of AtaR, AtaR-AtaT or AtaR-AtaT with substitutions in AtaR. (**c**) Toxicity assay involving AtaR-AtaT and mutants of ataR at the position of α-helix α2 that prevents the dimerization of AtaT.(**d-f**) Gating strategy representative example (P*ata*_ *AtaR-AtaT*) of the flow cytometry data analysis. In each case we analysed 75,000 events. Green fluorescence was measured with a blue laser (488 nm) and a 530/30 emission filter. Identical analyses were applied to all flow cytometry data. (**d**) Forward and side scatter density plots were used to identify the bacterial population and exclude debris. (**e**) Side scatter height versus side scatter area density plots were used to identify singulets and exclude doublets or triplets. (**f**) Green fluorescence histograms were used to identify fluorescent negative and fluorescent positive populations.

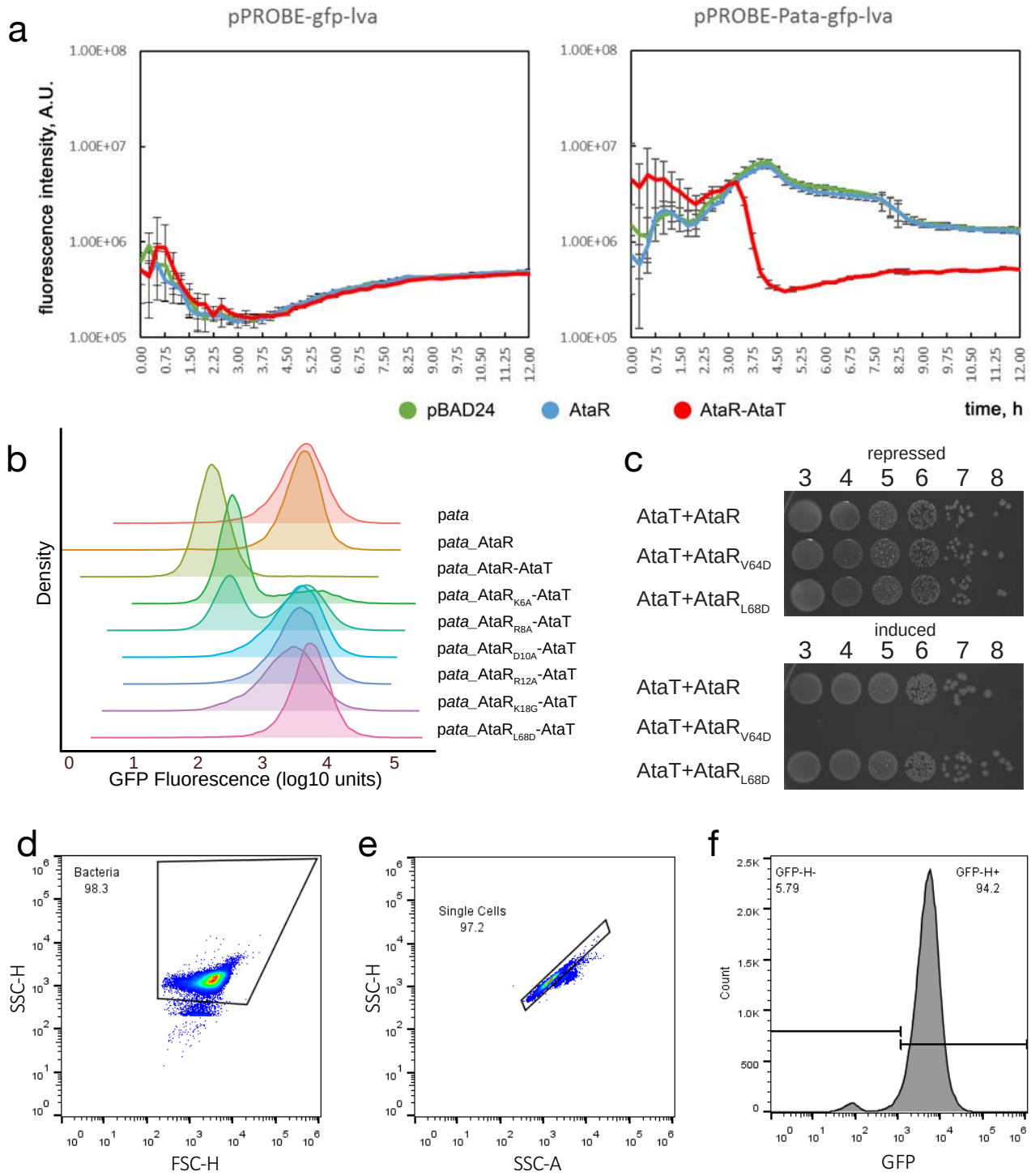
a
pPROBE-gfp-lva
pPROBE-Pata-gfp-lva
fluorescence intensity, A.U.
1.00E+08
1.00E+07
1.00E+06
1.00E+05
0.00 0.75 1.50 2.25 3.00 3.75 4.50 5.25 6.00 6.75 7.50 8.25 9.00 9.75 10.50 11.25 12.00
pBAD24
AtaR
AtaR-AtaT
time, h
b
Density
pata
pata_AtaR
pata_AtaR-AtaT
pata_AtaR$_{K6A}$-AtaT
pata_AtaR$_{R8A}$-AtaT
pata_AtaR$_{D10A}$-AtaT
pata_AtaR$_{R12A}$-AtaT
pata_AtaR$_{K18G}$-AtaT
pata_AtaR$_{L68D}$-AtaT
0 1 2 3 4 5
GFP Fluorescence (log10 units)
c
repressed
3 4 5 6 7 8
AtaT+AtaR
AtaT+AtaR$_{V64D}$
AtaT+AtaR$_{L68D}$
induced
3 4 5 6 7 8
AtaT+AtaR
AtaT+AtaR$_{V64D}$
AtaT+AtaR$_{L68D}$
d
Bacteria
98.3
SSC-H
FSC-H
e
Single Cells
97.2
SSC-H
SSC-A
f
GFP-H-
5.79
GFP-H+
94.2
Count
2.5K
2.0K
1.5K
1.0K
500
0
GFP

Supplementary Fig. 8. AtaRT binding to a mutated operator. EMSA assay of the binding of AtaRT to a mutated version of Opr_{47}. The assay shows that substitution of C6, G7 and G8 in the operator sequence (Supplementary Table 2), results in a significant decrease in binding to the AtaRT complex.

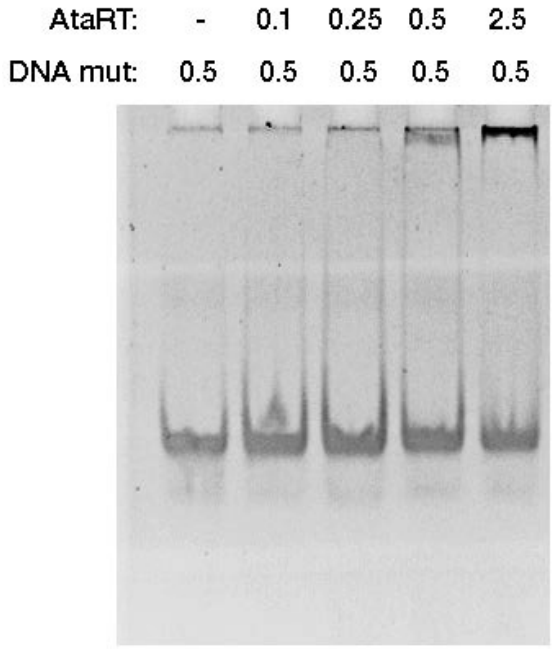

Supplementary Fig. 9. A secondary AtaR-AtaT interaction prevents dimerization and defines the repressor architecture. In the repressor complex, the AtaR IDR places the symmetry axis of both AtaR dimers ~32 Å apart, matching the pitch of B-DNA and facilitating the interaction of both dimers with the consecutive major grooves of the operator. The dimensions of this rhomboid structure are determined by α–helices α1 and α2 of AtaR and are reminiscent the way the phage repressor Arc binds to its operator.